Article

Microfabrication of Three-Dimensional Bioelectronic Architectures

Ryan T. Hill, Jennifer L. Lyon, Richard Allen, Keith J. Stevenson, and Jason B. Shear

J. Am. Chem. Soc., **2005**, 127 (30), 10707-10711• DOI: 10.1021/ja052211f • Publication Date (Web): 06 July 2005

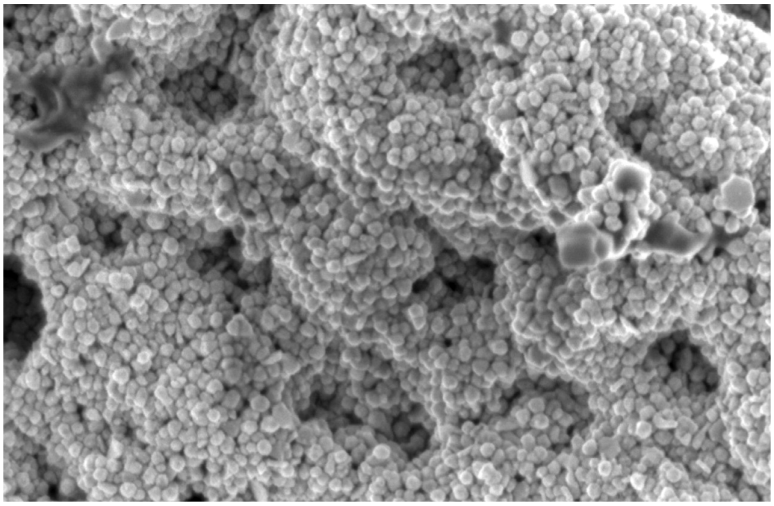

J|A|C|S
ARTICLES
Published on Web 07/06/2005

Microfabrication of Three-Dimensional Bioelectronic Architectures

Ryan T. Hill, Jennifer L. Lyon, Richard Allen, Keith J. Stevenson,* and Jason B. Shear*

Contribution from the Department of Chemistry and Biochemistry, University of Texas, 1 University Station A5300, Austin, Texas 78712

Received April 6, 2005; E-mail: jshear@mail.utexas.edu; stevenson@mail.cm.utexas.edu

Abstract: The functionality and structural diversity of biological macromolecules has motivated efforts to exploit proteins and DNA as templates for synthesis of electronic architectures. Although such materials offer promise for numerous applications in the fabrication of cellular interfaces, biosensors, and nanoelectronics, identification of techniques for positioning and ordering bioelectronic components into useful patterns capable of sophisticated function has presented a major challenge. Here, we describe the fabrication of electronic materials using biomolecular scaffolds that can be constructed with precisely defined topographies. In this approach, a tightly focused pulsed laser beam capable of promoting protein photocross-linking in specified femtoliter volume elements is scanned within a protein solution, creating biomolecular matrices that either remain in integral contact with a support surface or extend as free-standing structures through solution, tethered at their ends. Once fabricated, specific protein scaffolds can be selectively metallized via targeted deposition and growth of metal nanoparticles, yielding high-conductivity bioelectronic materials. This aqueous fabrication strategy opens new opportunities for creating electronic materials in chemically sensitive environments and may offer a general approach for creating microscopically defined inorganic landscapes.

Introduction

The ability of biological macromolecules to direct growth and organization of inorganic materials offers valuable opportunities for materials synthesis. Studies of natural biomineralization processes have inspired efforts to specify the structure of inorganic materials over many length scales, from quantum dots with well-defined crystallinity to large single crystals of calcium carbonate.[1,2] Recently, several strategies have been explored for using macromolecules to scaffold electronically conductive metallic components within aqueous solutions, a goal that could provide routes for fashioning new electrochemical architectures, nanoelectronic components, and cellular interfaces.

In these approaches, surface-adhered biofilaments (DNA[3−5] and polyproteins such as amyloid fibers,[6] peptide nanotubes,[7] and F-actin[8]) have been used as templates to grow metallic "biowires" through the catalytic reduction of copper, gold, and silver ions. Metallization has been initiated both directly from electrostatically associated ions or by covalently bound metal nanoparticle seeds. Although such procedures have yielded wires and radial dimensions as small as $\sim 0.1\ \mu$m with conductivities of $\sim 10^4$ S cm^{-1}, the arrangement of such materials into functional electronic patterns faces severe challenges.

In this report, we describe a strategy for constructing both surface-adherent and free-standing biomolecular scaffolds for electronic components with submicrometer, three-dimensional control. Here, proteins are photocrosslinked into controllably placed matrices that display high-binding capacities for functionalized metal nanoparticles; decoration of protein structures with nanoparticle seeds followed by reductive metallization yields hybrid materials that are highly conductive. By building protein-based structures using a direct-write process based on scanning multiphoton excitation (MPE), matrices can be fabricated with feature sizes that range from hundreds of nanometers to more than 1 mm and that may either remain in integral contact with a support surface or extend tens of micrometers into free solution.

Experimental Section

Reagents and Materials. Bovine heart cytochrome *c* (cyt *c*; Sigma-Aldrich, St. Louis, MO, C3131), avidin (Molecular Probes, Eugene, OR, A-887), and flavin adenine dinucleotide (FAD; Sigma-Aldrich, F-6625) were stored desiccated at −20 °C. Horse skeletal muscle myoglobin (Sigma-Aldrich, M-0630), bovine serum albumin (BSA; Equitech-Bio, Kerrville, TX, BAH64-0100), and methylene blue (Sigma-Aldrich, M-4159) were stored undesiccated at −20 °C, 4 °C, and room temperature, respectively. A concentrated stock solution of fluorescein-biotin (Molecular Probes, B-1370) in DMSO was stored

(1) Seeman, N. C.; Belcher, A. B. *Proc. Natl. Acad. Sci. U.S.A.* **2002**, *99*, 6451−6455.
(2) Aizenberg, J.; Muller, D. A.; Grazul, J. L.; Hamann, D. R. *Science* **2003**, *299*, 1205−1208.
(3) Monson, C. F.; Woolley, A. T. *Nano Lett.* **2003**, *3*, 359−363.
(4) Braun, E.; Eichen, Y.; Sivan, U.; Ben-Yoseph, G. *Nature* **1998**, *391*, 775−778.
(5) Keren, K.; Krueger, M.; Gilad, R.; Ben-Yoseph, G.; Sivan, U.; Braun, E. *Science* **2002**, *297*, 72−75.
(6) Scheibel, T.; Parthasarathy, R.; Sawicki, G.; Lin, X.; Jaeger, H.; Lindquist, S. L. *Proc. Natl. Acad. Sci. U.S.A.* **2003**, *100*, 4527−4532.
(7) Reches, M.; Gazit, E. *Science* **2003**, *300*, 625−627.
(8) Patolsky, F.; Weizmann, Y.; Willner, I. *Nat. Mater.* **2004**, *3*, 692−695.

at 4 °C. Catalytic gold enhancement solution was purchased from Nanoprobes (Yaphank, NY, 2112), and solutions of gold nanoparticles (~5 nm diameter) decorated with biotinylated BSA (b-BSA), biotinylated horseradish peroxidase (b-HRP), and unmodified HRP were purchased from EY Labs (San Mateo, CA, GB-01, GB-02, GP-03); each solution was stored at 4 °C. All reagents were used as received. H_2O used in all experiments was purified using a Barnstead NANOpure system (resistance, >18 MΩ). Glass coverslips (No. 1 thickness) were purchased from Erie Scientific (Portsmouth, NH).

Photolithographic Modification of Coverslips. Coverslips were coated with indium tin oxide (ITO; Metavac, Inc., Holtsville, NY) and patterned using standard photolithographic methods, yielding nonconductive barriers of bare glass (generally, 50−100 μm) between conductive regions of ITO. In this procedure, ITO coverslips (coating thickness, ~100−200 nm) were spin-coated with 1,1,1,3,3,3-hexamethyldisilazine (HMDS, Sigma) at 5000 rpm for 30 s, followed by the positive photoresist, AZ 5214E (5000 rpm for 60 s). Coated coverslips were prebaked at 120 °C for 80 s before being masked with an aluminum stencil (UTZ Technologies, San Marcos, CA) and exposed to UV radiation (460-W lamp for 15 s; ABM Instruments, Santa Barbara, CA). After exposure, coverslips were treated immediately with a 20% solution of developer (AZ 400K diluted in H_2O). ITO was etched in 1:3 HCl/HNO_3 solution for 120 s and was cleaned from coverslips by extended rinses with H_2O, acetone, and 2-propanol.

Multiphoton Fabrication. Before use, patterned coverslips were subjected to three rinses with each of the following: 2-propanol, ethanol, and an aqueous buffer containing 18 mM phosphate and 0.1 M sodium perchlorate (pH 7.4). In most cases, surface adsorption was reduced by soaking coverslips for 10 min in phosphate/perchlorate buffer containing 200 mg/mL BSA protein and rinsed 10 times with the buffer to be used for crosslinking. Protein matrices typically were fabricated using protein solutions in a pH 7.4 buffer using either FAD or methylene blue as a photosensitizer; for conductivity studies, cyt *c* was crosslinked without addition of a separate photosensitizer. Relatively high concentrations of protein (generally, 100−200 mg/mL) were found to provide the most reproducible fabrication of matrices.

Crosslinked protein structures were written on a Zeiss Axiovert (inverted) microscope using a femtosecond titanium:sapphire (Ti:S) laser (Spectra Physics, Mountain View, CA) typically tuned to 740 nm. The laser output was adjusted to approximately fill the back aperture of a high-power objective (Zeiss Fluar, 100×/1.3 numerical aperture, oil immersion); average laser powers entering the microscope were 20−40 mW. Photocrosslinked protein structures were created by raster scanning the focused laser beam within the focal plane using galvanometer-driven mirrors (BioRad MRC600 confocal scanner). In some instances, a motorized xy-stage was used to translate the position of the sample at ~3 μm/s as the beam was raster scanned, an approach capable of creating lanes of crosslinked protein that extend over (millimeter) distances ultimately limited by the stage travel. After protein crosslinking, structures were rinsed 30 times with H_2O. In circumstances where methylene blue or FAD was used, fluorescence measurements indicated that residual photosensitizer concentrations within matrices were low, although quantitative measurements of these species have not been performed.

Diagonal cables (i.e., extending both laterally along the optical axis) were fabricated between opposing glass coverslips spaced ~80−100 μm using Scotch Double Sided Tape (3M, St. Paul, MN). The focus of an Olympus 40×/0.95 numerical aperture Plan Apo objective was translated from the bottom surface of the top coverslip to the top surface of the bottom coverslip through a solution containing 400 mg/mL avidin, 0.6 mM methylene blue, 0.1 M NaCl, and 20 mM HEPES (pH 7.4). Generally, additional surface-adherent protein matrix was fabricated from the positions at which a cable contacted each coverslip, thereby increasing contact area and tethering stability. Cables were washed by displacing the crosslinking solution with H_2O (four reaction volumes, ~80 μL total). In some cases, cables were subsequently labeled using 1 μM fluorescein biotin.

Gold Nanoparticle Deposition and Enhancement. Structures were incubated with protein-coated gold nanoparticles for 0−10 min using the 2 mM borate buffer in which nanoparticles were supplied. Following nanoparticle exposure, matrices were rinsed another 30 times with H_2O. A gold enhancement solution (ca. pH 7) capable of catalytic reduction of gold onto nanoparticle seeds was applied to structures for ~13 min. Before characterization, samples were dehydrated by using five 10-min sequential washes (2:1 EtOH/H_2O; 2 × 100% EtOH; 1:1 EtOH:HMDS; 100% HMDS; all solutions vol:vol) and allowed to air-dry for periods of between 20 min and several days. In five separate negative control experiments, patterned ITO coverslips were treated with the same protein/photosensitizer solution used for fabrication of cyt *c* matrices but were not exposed to focused laser light. After removal of protein solution and rinsing, control coverslips were incubated with protein-coated nanoparticles and gold-enhancement solution in the same manner described for photofabrication samples.

Materials Characterization. Tapping-mode atomic-force microscopy (AFM) measurements were made using a Digital Instruments Dimension 3100 microscope in combination with a Nanoscope IV Controller (Veeco Metrology, Santa Barbara, CA). All measurements were obtained using uncoated, n-doped Si SPM probes (cantilever length, 125 μm; resonant frequency, 300 kHz; spring constant, 40 N/m; model MPP-11100, Nanodevices, Inc., Santa Barbara, CA). In some cases, metallized protein structures were severed using a focused ion beam (FIB; FEI-Strata DB235, Hillsboro, OR) operated using a beam current of 100 pA. Scanning electron micrograph (SEM) data were obtained from a LEO 1530 scanning electron microscope operating at an accelerating voltage of 3 keV with an 8-mm working distance and using magnifications of 1700−25 000×. In some cases, images were captured using an in-lens annular detector. Current−voltage data were collected using a Karl Suss PM5 probe station coupled to an Agilent 4145B semiconductor parameter analyzer. Tungsten filaments (2-μm radius) were used to probe the structures. In some studies, conductivity measurements were acquired using a CH Instruments 440 potentiostat (Austin, TX) interfaced to a PC. Transmission images of intact and severed protein wires were obtained using a Photometrics CoolSnap HQ CCD digital camera (Tuscon, AZ) mounted to the Axiovert fabrication microscope and interfaced to Metamorph imaging software (Universal Imaging Corporation, version 6.2, Downingtown, PA). Confocal images were acquired using a Leica SP2 AOBS confocal microscope outfitted with a 40× plan-apo 1.25 numerical aperture UV objective; fluorescein-biotin fluorescence was imaged on this system using the 488-nm line from an argon-ion laser and a FITC filter set.

Results and Discussion

Crosslinking of protein-residue side chains can be promoted by type I (direct radical) and type II (oxygen-dependent) photosensitizers[9,10] and has been controlled using near-infrared MPE to create rugged, surface-adherent matrices that can retain functionality of their protein constituents.[11−13] Nonlinear photosensitizer excitation restricts the reaction both radially and axially, resulting in a protein crosslinking volume element that can be less than 1 fL. By translating the relative position of the focus across a coverslip immersed in a solution of protein and photosensitizer, a continuous matrix can be fabricated with

(9) Spikes, J. D.; Shen, H. R.; Kopeckova, P.; Kopecek, J. *Photochem. Photobiol.* **1999**, *70*, 130−137.
(10) Verweij, H.; Van Steveninck, J. *Photochem. Photobiol.* **1982**, *35*, 265−267.
(11) Pitts, J. D.; Campagnola, P. J.; Epling, G. A.; Goodman, S. L. *Macromolecules* **2000**, *33*, 1514−1523.
(12) Pitts, J. D.; Howell, A. R.; Taboada, R.; Banerjee, I.; Wang, J.; Goodman, S. L.; Campagnola, J. *Photochem. Photobiol.* **2002**, *76*, 135−144.
(13) Kaehr, B.; Allen, R.; Javier, D. J.; Currie, J.; Shear, J. B. *Proc. Natl. Acad. Sci. U.S.A.* **2004**, *101*, 16104−16108.

feature sizes as small as ~250 nm. In the current studies, a Ti:S laser beam (740 nm) was used to excite FAD and methylene blue, molecules that act as photosensitizers to promote crosslinking of soluble proteins. In addition, we have found that cyt *c*, a heme protein, can efficiently photosensitize its own crosslinking. (The possibility exists that physical condensation processes may accompany covalent chemical crosslinking in the formation of cyt *c* matrices.)

Although protein matrices can maintain highly specific chemical interactions,[12,13] we have adopted a strategy here to bind metal nanoparticles to protein matrices using electrostatic interactions. In this approach, gold nanoparticles were functionalized with a protein that has an isoelectric point (pI) significantly different from that of the matrix protein, with the solution buffered at a pH intermediate to the two pI values. In the basic solutions provided as supports for protein-coated nanoparticles (pH 8.8−9.0), planar structures created from cyt *c* (pI = 9.4)[14] showed a high capacity for binding nanoparticles coated with b-BSA (Figure 1a), a strongly acidic protein with a native pI of 4.8.[15] (Modification of proteins via biotinylation and cross-linking may alter isoelectric points.) Particles were bound at densities sufficient to completely envelop the matrix surface after reductive growth enlarged particles to ~50 nm. Pretreatment of b-BSA nanoparticles with avidin solution blocked their ability to associate with cyt *c* structures. Similarly high levels of b-BSA nanoparticle loading were achieved for structures composed of another basic protein, avidin (pI > 10),[16] and nanoparticles coated with HRP and b-HRP (principally the C isoform, native pI ≈ 8.5−9.0)[17] were bound by cyt *c* structures at comparable levels (specific avidin-biotin recognition may assist electrostatic binding in the association of biotinylated protein particles with avidin matrices).

Consistent with an electrostatic role in binding, structures fabricated from both myoglobin (pI ≈ 7) and BSA did not bind appreciable amounts of b-BSA nanoparticles. Moreover, treatment of cyt *c* matrices (fabricated on ITO) with solution-phase BSA and photosensitizer before addition of b-BSA nanoparticles blocked nanoparticle association. Figure 1b demonstrates this selective metallization of desired protein matrices.

A key feature of multiphoton photofabrication is that supporting protein matrices can be constructed with well-defined topographies. Figure 2a,b demonstrates capabilities for fabricating and metallizing crosslinked protein cables that extend through solution, unsupported, for nearly 100 μm between two opposing coverslips. Crosslinked proteins can be written into a diverse range of geometries, with the complexity of patterns limited primarily by the sophistication of scanning instrumentation and software. We have fabricated structures of various dimensionality, including parallelograms (Figure 2c), helices, microparticles, and arcs that loop from a surface.[13]

To examine the ability of metallized protein matrices to electronically conduct, ITO substrates were patterned with ~50−100 μm insulating breaks of bare glass; cyt *c* structures were fabricated across these electronic barriers, overlapping at their ends with the conductive ITO pads. Ohmic scaling

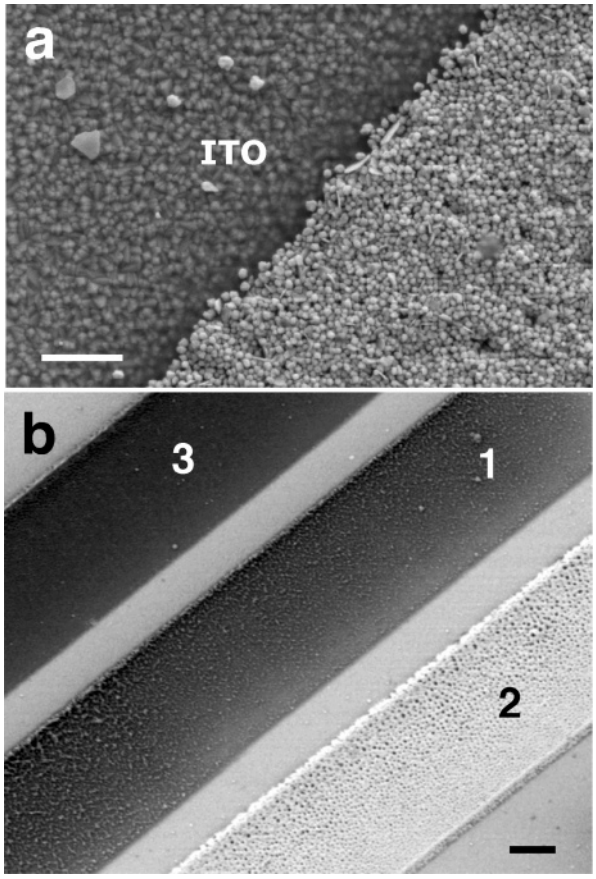

Figure 1. Specific, high-density metallization of matrices composed of photocrosslinked cytochrome c (cyt *c*). (a) SEM showing the interface between a metallized cyt *c* structure and an ITO-coated glass substrate. Scale bar, 0.5 μm. The graininess of the ITO coating can be clearly seen, as well as a few bright, nearly spherical gold particles scattered on the surface. (b) SEM of crosslinked BSA (lane 1), cyt *c* (lane 2), and cyt *c* blocked with BSA/photosensitizer (lane 3; blocking performed using 200 mg/mL protein in a methylene blue/HEPES solution for ~5−10 min) after application and reductive growth of gold nanoparticles. Structures were fabricated on an ITO substrate; nonconductive regions (i.e., the BSA and blocked cyt *c* lanes) appear dark in this image. Scale bar, 5 μm. For all structures fabricated in (a) and (b), cyt *c* was photocrosslinked in a solution containing 100 mg/mL cyt *c*, 18 mM phosphate buffer, 0.1 M sodium perchlorate, and 4.5 mM FAD; BSA structures were prepared in 200 mg/mL BSA, 20 mM HEPES, 0.1 M NaCl, and 0.6 mM methylene blue.

measurements were performed on representative metallized cyt *c* structures (Figure 3a). Here, tungsten probes were placed in contact with ITO adjacent to the ends of the protein wires. From these data and measurements on three additional test samples, apparent conductivities for structures fabricated across insulating gaps ranged from 6 to 14 S cm^{-1}; generally, structures displayed consistent I−V responses for days. Importantly, conductivities were nearly zero unless nanoparticles were both applied to structures and subjected to reductive growth. Following initial *I*−*V* measurements, wires could be severed using FIB milling. Figure 3b shows a FIB cut made through a wire, a disruption that virtually eliminated current flow. Although some nonspecific deposition of gold can be seen in the vicinity of this structure, FIB disruption of the matrix decreased conductivity by more than 10^6-fold. (e.g., at 100 mV the severed structure supported a current of 2 pA versus 50 μA in an intact structure).

As further confirmation that current responses could not be attributed to nonspecific adsorption of protein (and subsequent

(14) Righetti, P. G.; Caravaggio, T. *J. Chromatogr.* **1976**, *127*, 1−28.
(15) Peters, T., Jr. *Adv. Protein Chem.* **1985**, *37*, 161−245.
(16) Melamed, M. D.; Green, N. M. *Biochem. J.* **1963**, *89*, 591−599.
(17) Yamazaki, I.; Nakajima, R. In *Molecular and physiological aspects of plant peroxidases*; Greppin, H., Penel, C., Gaspar, T., Eds.; University of Geneva Press: Geneva, Switzerland, 1986.

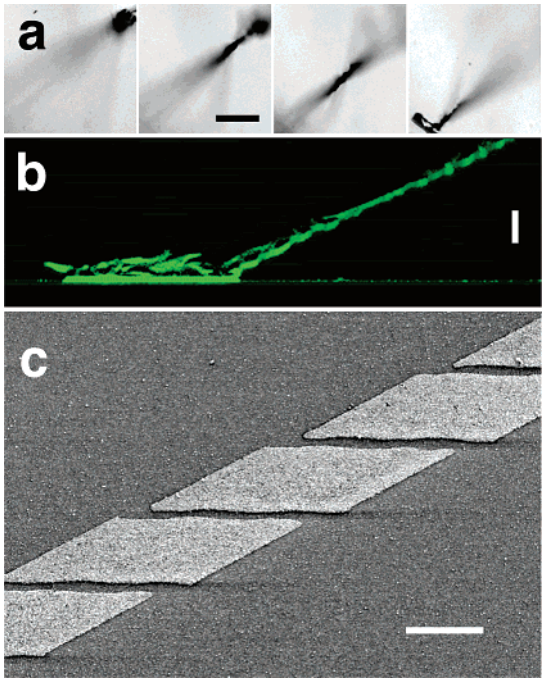

Figure 2. Metallized protein architectures. (a) Transmission images of an avidin cable that extends between two spaced glass coverslips. In the left panel, the lower surface of the upper coverslip is in focus; the subsequent panels focus downward in steps of 24, 24, and 28 μm. The cable's high optical density is caused by reductively grown gold nanoparticles. Scale bar, 40 μm. (b) Confocal reconstruction of an avidin cable labeled with fluorescein biotin and gold nanoparticles, but not subjected to reductive gold growth. The top tethering region of this cable extended just beyond the depth of focus. Scale bar, 20 μm. In parts (a) and (b), structures were fabricated by scanning the stage laterally at several micrometers per second while simultaneously translating the depth of the focal point within the sample solution. (c) SEM of metallized cyt *c* parallelograms fabricated on an ITO coverslip. Scale bar, 10 μm.

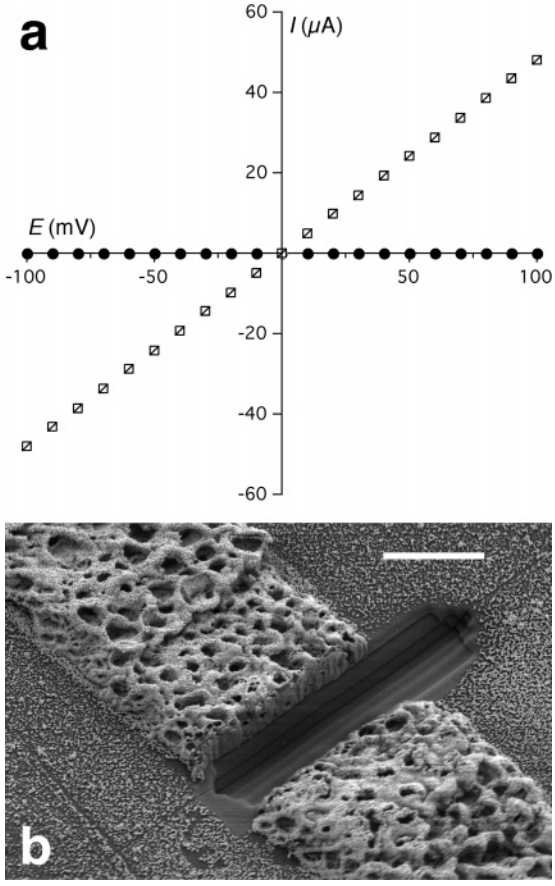

Figure 3. Electronic characterization of metallized protein architectures. (a) Current−potential measurements on a representative sample in which a metallized cyt *c* matrix spanned an insulating gap (~68 μm) between ITO electrodes (⍁) and after the matrix was severed (●). (b) SEM of the metallized cyt *c* matrix after severing with a FIB. Scale bar, 5 μm. Solutions used to fabricate protein matrices in parts (a) and (b) contained 200 mg/mL cyt *c* with no additional photosensitizer.

gold deposition) on the glass surface, we conducted control experiments in which patterned ITO slides were subjected to identical solutions and procedures as protein matrix samples, with the exception that protein photocrosslinking was not performed. Currents measured for these controls were ~1 pA at an applied potential of 100 mV and did not scale with potential.

Interestingly, significant differences were found in photocross-linking cyt *c* on glass and ITO surfaces: the fabrication process on glass is less controllable, typically requiring greater laser powers and higher concentrations of cyt *c*. As can be seen from a comparison of Figures 1 and 3b, cyt *c* matrices on glass are less uniform and more porous than those patterned on ITO. AFM analysis indicated that heights of metallized cyt *c* matrices on insulating glass regions ranged from ~1.5 to 3.0 μm (compared to ~700 nm on ITO). Although the causes of these differences are not certain, we speculate that decreased dissipation of local heating on glass (dependent on thermal conductivity) plays a role in determining matrix structure, as diffusion and convection should result in more rapid depletion of reactive photoproducts from the multiphoton focal volume. Notably, matrices composed of various other proteins, including avidin, could be fabricated more controllably on glass substrates than structures formed from cyt *c*. Although avidin matrices efficiently bound gold nanoparticles, they were not used in initial conductivity studies because of higher nonspecific adsorption of avidin to glass and, hence, greater background binding of nanoparticles.

In these initial measurements of metallized cyt *c* conductivity, contact resistance between the protein matrix and ITO appears to be a limiting factor. To evaluate this effect, several additional samples were characterized by placing the tungsten probes in direct contact with metallized cyt *c* structures. Although probe contact caused some damage to protein matrices, measured conductivities increased to $\sim 10^3$ S cm^{-1}, nearly 100-fold greater than that determined with the probes placed on the ITO surfaces. Another source of error in calculating conductivities is our simplifying assumption that matrices are solid (i.e., contain no void volume), a poor approximation given the high level of porosity of cyt *c* structures fabricated for conductivity measurements (Figure 3b).

In the current studies, we have examined electrical conductivity measurements obtained ex situ (i.e., on dried, metallized photocrosslinked cyt *c* matrices) and have not assessed the extent to which native cyt *c* structure may be compromised during matrix formation (e.g., due to thermal or photochemical processes). Nevertheless, crosslinking studies using avidin, a protein that retains biotin-binding activity in matrices, demonstrate that metallization is not generally dependent on protein denaturation. Electrochemical studies, outside the scope of this report, also are underway to probe direct electron-transfer

properties of (unmetallized) photocrosslinked cyt *c* and other heme-containing proteins on electrode surfaces and immersed in buffered aqueous solutions.

Unlike earlier approaches for templating metals with biomolecules, the current strategy can be used to construct scaffolds with precise spatial control in three dimensions, offering new opportunities to construct advanced bioelectronic architectures. Because metallized protein matrices can be fabricated using mild aqueous conditions and with a broad range of geometries, protein-based microfabrication can be performed in chemically sensitive and mechanically confined environments. We are adapting these procedures for compatibility with cultures of neurons[13] and other cell types, a goal that would substantially expand capabilities for constructing in situ bioelectronics for monitoring and stimulating biological processes. Because proteins have been shown to effectively template materials as varied as quantum dots,[1] hydroxyapatite, and silica,[18] the strategy described in this report may portend a general approach for creating microscopically defined inorganic landscapes.

Acknowledgment. We thank UTZ Tech. for donation of photolithography stencils, B. Kaehr for useful discussions, and R. Williams, R. Nielson, D. Romanovicz, and Y.-L. Loo for technical advice and assistance. We acknowledge the Welch Foundation (F-1331, F-1529), the NSF (Grant 0317032), and SPRING for support, and the Center for Nano- & Molecular Science/Technology for FIB instrumentation. J.B.S. is a fellow in the Institute for Cellular & Molecular Biology.

JA052211F

(18) Chunmei, L.; Kaplan, D. L. *Curr. Opin. Solid State Mater. Sci.* **2003**, *7*, 265−271.